Proc. Natl. Acad. Sci., India, Sect. A Phys. Sci. (July–September 2023) 93(3):445–450
https://doi.org/10.1007/s40010-023-00829-9

RESEARCH ARTICLE

Investigation of Defect-Driven Memristive and Artificial Synaptic Behaviour at Nanoscale for Potential Application in Neuromorphic Computing

Rupam Mandal[1,2] · Dilruba Hasina[1,2] · Aparajita Mandal[1] · Tapobrata Som[1,2]

Received: 25 July 2022 / Revised: 17 May 2023 / Accepted: 24 May 2023 / Published online: 22 June 2023
© The Author(s), under exclusive licence to The National Academy of Sciences, India 2023

Abstract The need for nano-sized memristive devices as synaptic emulators is increasing day-by-day to build neuromorphic devices on a chip with a large integration density. Therefore, nanoscale fabrication and subsequent device assessment are exigent to make further advancements in the field. In this report, by employing atomic force microscopy, we demonstrate highly dense electronic nano-synapses in filamentary metal oxide-based memristors, wherein the tip works as one of the electrodes. Different metal oxide-based memristors with varying defect concentrations have been studied to demonstrate the efficacy of atomic force microscopy-based local probe techniques in extracting the defect-dependent performance metrics of the same at nanoscale. Some of the basic biological synaptic characteristics such as potentiation/depression and spike's property-dependent plasticities are accessed through different pulsed measurements in conductive atomic force microscopy mode. The current maps acquired using conductive atomic force microscopy measurements on the films confirm the filamentary resistive switching behaviour to prevail and point towards a possible decrease in the operating voltage with an increase in defects density. Kelvin probe force microscopic analyses, on the other hand, suggest that to improve the switching stability, resistivity of the active medium needs to be optimized. Overall, our results substantiate the efficacy of local probe microscopy-based methods to optimize the performance of memristive synapses at nanoscale for potential application in neuromorphic computing.

Keywords Resistive switching · Artificial electronic synapse · Neuromorphic computing · Ion-implantation · Cu-doped ZnO · TiO_x

1 Introduction

Resistive switching (RS) devices are being extensively studied due to their potential to overcome the von Neumann bottleneck for facilitating in-memory computing [1, 2]. Besides that machine learning and other neural network-based in-memory computing systems are also widely exploiting the RS devices to mimic the basic bio-synaptic functionalities [3, 4], wherein the memristors work as artificial synapses. As a future technology requirement, high-density integration of such artificial electronic synapses necessitates scalability of the devices down to nanometers [5]. To date, RS devices are mostly investigated at bulk level, inferences drawn from which may not be appropriate to nanoscale devices [6]. For example, it has been observed that requirement of forming voltage increases with a decrease in device size [7]. Nevertheless, the phenomena regulating their RS behaviour such as filament formation/annihilation [8], local phase variation [9] or ferroelectric domain switching [10] are confined at nanoscale, which therefore, makes it necessary to perform nanoscale analysis to fully comprehend the underlying mechanism. Interestingly, by exploiting atomic force microscopy (AFM), wherein the nano-sized AFM tip (~25 nm radius of curvature) works as one of the electrodes, one can investigate the device scalability and local electrical properties at nanoscale without the complexity of fabricating

Rupam Mandal and Dilruba Hasina have contributed equally to this work.

✉ Tapobrata Som
tsom@iopb.res.in

1 SUNAG Laboratory, Institute of Physics, Sachivalaya Marg, Bhubaneswar 751 005, India

2 Homi Bhabha National Institute, Training School Complex, Anushakti Nagar, Mumbai 400 094, India

several small devices with ultra-high packing density [11, 12].

In this paper, we demonstrate synaptic functionalities in transition metal oxide (TMO)-based filamentary memristors using different versatile modes of AFM. In this regard, most of the TMOs, such as ZnO, TiO_2, NiO, and HfO_2, are preferred candidates due to their adaptability to the deviation in their local intrinsic/extrinsic defect landscape that promotes the formation of conducting channels/filaments, which largely govern their memristive/synaptic functionalities [13–16]. We investigate the influence of defect modification on memristive and synaptic properties in two types of metal oxide [viz. ZnO:Cu (2 wt%) (CZO) and TiO_x ($x < 2$)]-based memristors at nanoscale. The CZO films are modified *in situ* by incorporating O_2 gas of varying flow rates during the film growth to compensate for the excess amount of oxygen vacancy (O_V) concentration within the films [17]. The TiO_x films, on the other hand, are subjected to post-deposition implantation by Ar^+-ions of varying fluences with the aim to introduce increased density of O_V defects [11, 18]. A detailed AFM-based local probe analysis reveals the role of CZO film's resistivity in facilitating stable RS operation, whereas defect modification in TiO_x films by ion implantation reduces the operating voltages, affirming their potential for energy-efficient devices. We further demonstrate forming-free resistive switching along with emulation of the fundamental bio-synaptic functionalities in both devices at nanoscale that not only marks their potential to develop artificial neural networks with ultra-high density integration for in-memory computation [5, 11], but also establishes AFM as a versatile tool for optimizing nano-sized memristors and electronic synapses.

2 Experimental Details

CZO and TiO_x films were grown on ultrasonically cleaned ITO/glass (Merck) and $Pt/TiO_2/SiO_2/Si$ (platinized-Si, Radiant Technology, UK) substrates, respectively, using a pulsed laser deposition (PLD) system at room temperature (RT). The PLD has several advantages including versatility, control over the growth rate, stoichiometric transfer and unlimited degrees of freedom in the ablation geometry compared to other deposition techniques [19]. In this study, a KrF excimer laser (wavelength: 248 nm, pulse duration: 20 ns, and repetition rate: 10 Hz) with a fixed laser energy density of 1.7 J cm^{-2} was employed to ablate a hot-pressed ceramic target of the respective material. To control the concentration of the intrinsic oxygen vacancy defects, two different methods are adopted. For CZO films, different O_2 flow rates (viz. 0, 5, and 10 SCCM) were introduced during deposition. On the other hand, the TiO_x films are implanted post-deposition by 5 keV Ar^+-ions at an incident angle of 45° with respect to the surface normal of the sample with different ion fluences in the range of $(0.5-3) \times 10^{17}$ ions cm^{-2} at RT using an electron cyclotron resonance (ECR)-based ion source at Institute of Physics, Bhubaneswar, India.

The thicknesses of the as-grown CZO and TiO_x films are 100 and 80 nm, respectively, as determined using a profilometer. The surface morphology of the films was studied by using tapping mode AFM (Asylum Research, Model: MFP-3D). Electrical measurements were performed using conductive atomic force microscopy (cAFM) with a conducting Ti/Ir-coated tip (ASYELEC.02-R2, Electric-lever, Olympus) having a radius of curvature ~ 25 nm, stiffness ~ 42 N m^{-1}, and a resonance frequency ~ 285 kHz. During the cAFM measurements, the bias was applied to the bottom electrodes (BE), while the cAFM tip was kept virtually grounded. In order to investigate the resistive switching properties of the metal oxide films, local current–voltage (*I-V*) measurements are performed using cAFM technique by placing the cAFM tip on a randomly chosen spot on the film. In this process, the cAFM tip works as a top electrode and ITO (Platinized-Si) as a bottom electrode, fulfilling the basic metal/insulator/metal (MIM) configuration for a two-terminal memristive device. The *I-V* measurements are carried out on a large number of randomly chosen spots on the films, which exhibit similar behaviours.

In addition, Kelvin probe force microscopy (KPFM) was performed in dual-pass tapping mode with a user-defined lift height of 40 nm to estimate the local work function of the films. All the measurements were carried out in a closed enclosure having very low humidity [12].

3 Results and Discussion

3.1 Memristive Performance of CZO Films

Figure 1a depicts the *I-V* characteristics of the CZO-based memristors grown under the oxygen flow rate of 10 SCCM. The *I-V* curves are acquired on a large number of randomly chosen point locations on the sample surface. From the figure, the SET process, i.e. a transition from the initial high resistance state (HRS) to a low resistance state (LRS) and subsequent RESET process (transition from LRS to HRS) are distinguishable. However, the RS loop for the film grown in the absence of any oxygen partial pressure (i.e. $p_{O2} = 0$ mbar) disappears within 3 cycles. Although not stable, the other film grown under an O_2 flow rate of 5 SCCM reflects improvement in the RS stability and a loop opening up to 20–30 cycles (data not shown). Interestingly, the device grown under 10 SCCM O_2 flow shows an impressive RS behaviour for more than 100 cycles. The inset in Fig. 1a shows the variations in the SET and RESET voltages for 100 RS cycles, ensuring the excellent stability

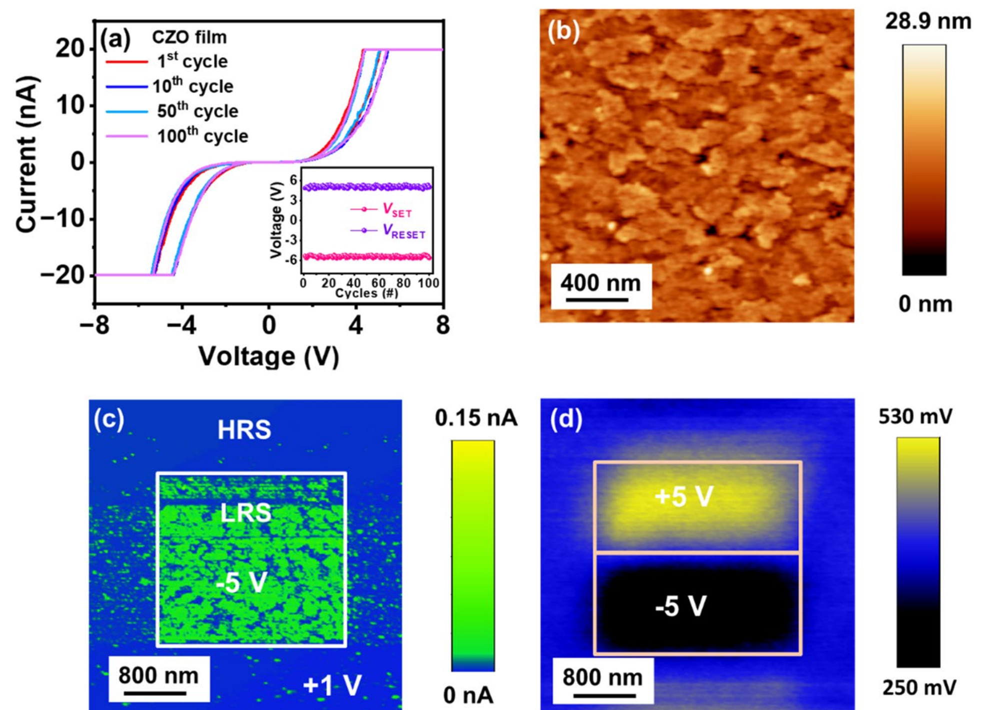

Fig. 1 **a** Depicts *I-V* curves for 100 sweep cycles at a single point location on the CZO film grown under an oxygen flow rate of 10 SCCM. The inset shows variations in SET/RESET voltages for 100 cycles. **b** Surface topography, and **c** local current map obtained by applying a write voltage (−5 V) and then a read voltage of + 1 V. **d** V_{CPD} map acquired after applying + 5 and −5 V successively to the AFM tip in contact mode, during KPFM measurements

of this device. The introduction of O_2 during the growth of CZO films compensates for the excessive defects present in the form of O_V, making the film more resistive that helps in improving the stability of the RS process [20]. In this respect, KPFM can be a useful tool to estimate the local work function and therefore, the resistivity of the films, which is an important metric for the stability of a device and charge transport across the hetero-junctions involved [21]. From KPFM analysis, the work function is observed to rise from 4.25 to 4.43 to 4.53 eV for the films grown under 0, 5, and 10 SCCM of O_2 flow rates, respectively. The systematic rise in work function, therefore, indicates an increase in the film resistivity (confirmed by four-probe measurements) when grown under increasing O_2 flow rates because of the compensation of intrinsic O_V defects that would otherwise increase the electron density in the conduction band of the film [20]. Here, it is important to mention that although the CZO films grown under higher O_2 flow rates exhibit stable resistive switching behaviour, the respective operating voltages increase with increasing O_2 flow rate (5.3–8–9.9 V for 10, 15 and 20 SCCM), which is not desirable for their practical applications. Therefore, the CZO films grown under 10 SCCM O_2 flow can be considered as the optimized ones in terms of switching stability and operating voltages [Fig. 1a].

Henceforth, we make use of this film for further investigations. The surface morphology image acquired using tapping mode AFM of this film shows a granular structure with a decent root mean square roughness of 2.5 nm [Fig. 1b]. For a clear visualization of the read/write operation on the optimized CZO film, a cAFM current map is acquired by scanning a 2 µm × 2 µm region using −5 V. This is a write process that decreases the resistance of the scanned region up to LRS. Then, a bigger area (4 µm × 4 µm) was scanned with a read voltage of +1 V. The higher current values observed in the region of writing clearly represent a successful write/read operation into the memristor [Fig. 1c]. It is worth mentioning here that each nano-sized conducting grain detected within the LRS region in Fig. 1c resembles one end of the channel/filament that spans from below the AFM tip location through the CZO active layer up to the bottom electrode (BE) [22, 23]. The presence of such conducting grains in the cAFM current map points towards a filamentary RS mechanism within the device [24]. In another useful application, KPFM can be exploited to get insights into the nature of charge storage capability (unipolar to bipolar) of any memristor. Here, we have employed field-induced KPFM measurements to record the contact potential difference (V_{CPD}) map of the film's surface. As shown in Fig. 1d, the biasing with different polarity of voltages (here ± 5 V) results in a noticeable increase (or decrease) in the V_{CPD} value in the respective regions, which confirms the bipolar charge storage capability of the CZO film under consideration [21, 22].

Next, we demonstrate the emulation of synaptic functionalities in the optimized CZO-based memristors by showing a possible analogy between a single electronic nano-synapse probed by cAFM and a biological synapse [Fig. 2a]. Here, the bottom ITO electrode works as a pre-synaptic neuron and the cAFM tip behaves as a post-synaptic neuron.

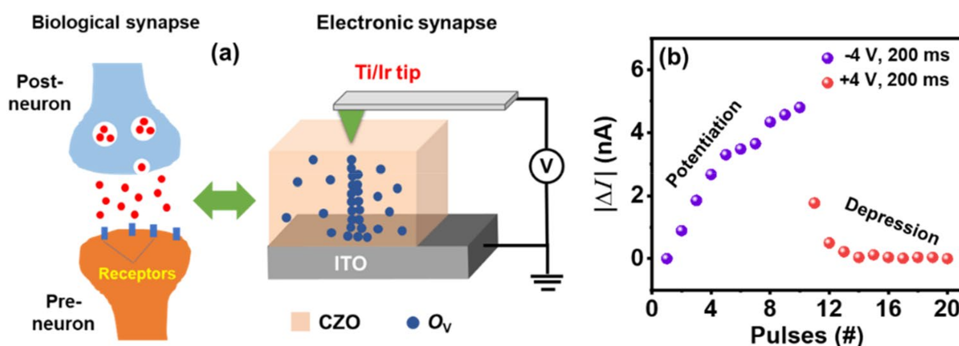

Fig. 2 **a** Schematic illustration of a CZO-based nanoscale electronic synapse in analogy to a biological synapse between two neurons. **b** The current response under 10 consecutive negative voltage pulses (−4 V, 200 ms) followed by 10 positive pulses (+4 V, 200 ms) with an interval of 10 ms, corresponding to potentiation and depression phenomena in a bio-synapse, respectively

Interestingly, the lateral scanning of the conducting tip inherently generates artificial nano-synapse (Ti/Ir tip/CZO/ITO) at the point of measurement on the film's surface, the conductance of which can be modulated under successive input electrical stimulations of different amplitudes, widths, and intervals. Figure 2b depicts the current response under ten identical negative (−4 V) and positive (+4 V) pulses having width and interval of 200 ms and 10 ms, respectively. The observed modulation in current ($\Delta I = I_N – I_1$; $N = 1$ to 10 denotes the pulse number) under the negative (positive) pulses shows an excellent analogy with the potentiation (depression) of a bio-synapse where the synaptic current level enhances (reduces) with pulse number. The observed potentiation phenomena in the present CZO memristors can be explained by means of current augmentation in subsequent pulses of the same polarity. In contrast, if consecutive depressing spikes are applied, dissolution of the localized filament-like conducting chains reduces the current with successive pulse numbers.

3.2 Memristive Performance of TiO_x Films

Figure 3a, b depict the cAFM current maps (acquired at an applied bias of + 1 V) corresponding to the as-grown and Ar^+-ion implanted TiO_x specimen (to the highest fluence), respectively, where the current conduction sites are clearly observed, confirming the filamentary RS mechanism similar to the CZO films. Further, the current map reveals an overall improvement in conductivity of the films with increasing ion

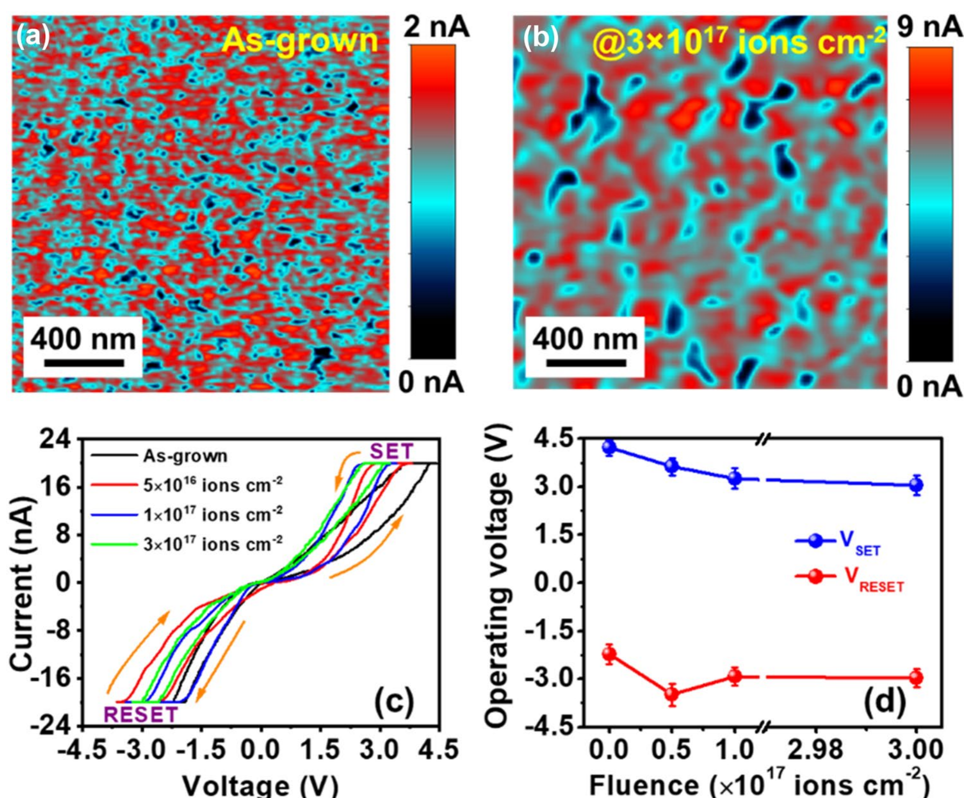

Fig. 3 **a**–**b** Show the current maps of as-grown and Ar^+-ion implanted TiO_x samples (to the highest fluence). **c** Variation in *I-V* characteristics and **d** operating voltages before and after implantation using different fluences

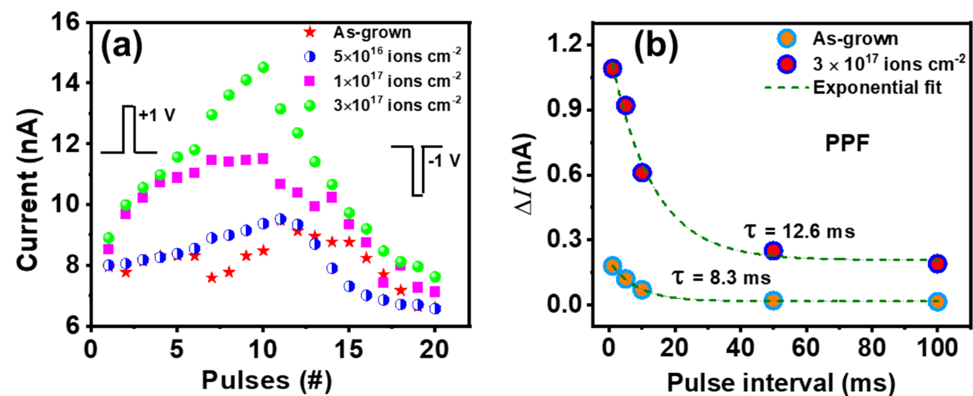

Fig. 4 **a** Potentiation and depression against pulse number under identical positive voltage pulse train (+1 V, width and duration: 1 ms) followed by a negative one (−1 V, width and duration: 1 ms) for as-grown and ion implanted films. **b** PPF behaviour of as-grown and ion-implanted (ion-fluence: 3×10^{17} ions cm^{-2}) films

fluence, which can be attributed to the fluence-dependent increase in O_V within the same [11].

To investigate the possible effects of ion implantation on RS performance, point *I-V* characteristics of as-grown and ion-implanted films are recorded with a cyclic voltage sweep from $0\rightarrow+5\rightarrow0\rightarrow-5\rightarrow0$ V (ramp rate of 0.2 V s^{-1}) using cAFM technique [Fig. 3c]. Interestingly, it is observed that with increasing ion fluence, the RS loops shift towards the lower operating voltages (cycle-to-cycle variation in operating voltages is indicated by the error bars) [Fig. 3d]. This implies that the ion-implanted films, particularly the ones implanted to the highest fluence, consume less power to execute RS operation. Similar to the CZO, these TiO_x memristors do not require electroforming.

Next, to examine the feasibility of the developed TiO_x memristors as electronic synapses, cAFM-based investigations are carried out following the same techniques as that of the CZO films discussed in Sect. 3.1. The variation in current under the application of a voltage pulse train (+1.0 V; width, Δd: 1 ms, and interval, Δ*t*: 1 ms) for as-grown and ion implanted films are shown in Fig. 4a. It is observed that the potentiation behaviour of the memristor improves with increasing ion fluence, which is an important parameter to determine the rate of learning of a synaptic device [11]. The generated nano-synapse corresponding to the highest fluence exhibited superior potentiation/depression behaviour compared to the other ones. Further, the paired-pulse facilitation (PPF) behaviour of as-grown and the one implanted to the highest ion fluence (i.e. at 3×10^{-17} ions cm^{-2}) are examined under pulse trains of varying intervals (amplitude: +1.0 V, width: 1 ms, intervals: 1, 5, 10, 50, and 100 ms). The PPF is calculated as (I_2—I_1), where I_1 and I_2 are the current response of the first and the second pulse, respectively. As shown in Fig. 4b, the PPF decreases exponentially when the pulse interval increases, similar to the bio-synapses. The exponential fitting of the experimental PPF data yields the value of decay constants (τ, values are mentioned in the respective figure). Here, it is interesting to note that the rate of decay (reciprocal of the decay constant) is slow for the implanted film than that of the as-grown one. A slower decay indicates the ability of a device to achieve faster learning with fewer training cycles.

4 Conclusion

We demonstrate memristive synapses at nanoscale in CZO and TiO_x− films exploiting different modes of AFM technique. A clear signature of defect modification either by changing *in situ* O_2 flow (in case of CZO) or by ion implantation using different fluences (in case of TiO_x) is inevitably present in all the acquired AFM data. The conductive mode AFM revealed forming-free and stable filamentary RS properties along with successful emulation of bio-synaptic functions in both types of films. On the other hand, KPFM analysis points towards reduced oxygen vacancy concentration within the CZO films that improves RS stability. The cAFM current maps suggest an increase in oxygen vacancy concentration after ion implantation, reducing the operating voltages, thereby making the RS operation of TiO_x more power efficient. Therefore, our approach to demonstrate forming-free memristors with synaptic functionalities at nanoscale proves to be highly suitable for developing next-generation high-density, power-efficient neuromorphic devices on a chip.

Declarations

Conflict of interest The authors declare that they have no conflicts of interest.

References

1. Ielmini D, Wong H-SP (2018) In-memory computing with resistive switching devices. Nat Electron 1:333–343

2. Wang J, Zhuge F (2019) Memristive synapses for brain-inspired computing. Adv Mater Technol 4:1800544
3. Ohno T, Hasegawa T, Tsuruoka T, Terabe K, Gimzewski JK, Aono M (2011) Short-term plasticity and long-term potentiation mimicked in single inorganic synapses. Nat Mater 10:591–595
4. Yan X, Qin C, Lu C et al (2019) Robust Ag/ZrO_2/WS_2/Pt memristor for neuromorphic computing. ACS Appl Mater Interfaces 11:48029–48038
5. Kumar M, Singh R, Kang H, Park JY, Kim S, Seo H (2020) Brain-like spatiotemporal information processing with nanosized second-order synaptic emulators; "solid-state memory visualizer." Nano Energy 76:105014
6. Lanza M, Wong HSP, Pop E, Ielmini D, Strukov D et al (2019) Recommended methods to study resistive switching devices. Adv Electron Mater 5:1800143
7. Hui F, Lanza M (2019) Scanning probe microscopy for advanced nanoelectronics. Nat Electron 2:221–229
8. Saini M, Kumar M, Mandal R, Mitra A, Som T (2021) White light modulated forming-free multilevel resistive switching in ZnO: Cu films. Appl Surf Sci 563:150271
9. Carboni R, Ielmini D (2019) Stochastic memory devices for security and computing. Adv Electron Mater 5:1900198
10. Boppidi PKR, Raj PMP, Challagulla S, Gollu SR, Roy S, Banerjee S, Kundu S (2018) Unveiling the dual role of chemically synthesized copper doped zinc oxide for resistive switching applications. J Appl Phys 124:1–10
11. Hasina D, Kumar M, Singh R, Mollick SA, Mitra A, Srivastava SK, Luong MA, Som T (2021) Ion beam-mediated defect engineering in TiO_x thin films for controlled resistive switching property and application. ACS Appl Electron Mater 3:3804–3814
12. Kumar M, Som T (2015) Structural defect-dependent resistive switching in Cu–O/Si studied by Kelvin probe force microscopy and conductive atomic force microscopy. Nanotechnology 26:345702
13. Ismail M, Mahata C, Kim S (2022) Electronic synaptic plasticity and analog switching characteristics in Pt/TiO_x/AlO_x/AlTaON/TaN multilayer RRAM for artificial synapses. Appl Surf Sci 599:153906
14. Kumar M, Ban DK, Kim SM, Kim J, Wong CP (2019) Vertically aligned WS_2 layers for high-performing memristors and artificial synapses. Adv Electron Mater 5:1900467
15. Kumar M, Lim J, Park JY, Kim S, Seo H (2020) Electric-field-induced healing of inanimate topographies: multistate resistive switching and nano-sized artificial synapse functionality. Appl Surf Sci 530:147190
16. Roy S, Niu G, Wang Q, Wang Y, Zhang Y et al (2020) Toward a reliable synaptic simulation using Al-Doped HfO_2 RRAM. ACS Appl Mater Interfaces 12:10648–10656
17. Huang HW, Kang CF, Lai FI, He JH, Lin SJ, Chueh YL (2013) Stability scheme of ZnO-thin film resistive switching memory: influence of defects by controllable oxygen pressure ratio. Nanoscale Res Lett 8:483
18. Nandi SK, Venkatachalam DK, Ruffell S, England J, Grande PL, Vos M, Elliman RG (2018) Room temperature synthesis of HfO_2/HfO_x heterostructures by ion-implantation. Nanotechnology 29:425601
19. Ogugua SN, Ntwaeaborwa OM, Swart HC (2020) Latest development on pulsed laser deposited thin films for advanced luminescence applications. Coatings 10:1078
20. Kim D, Jang JT, Yu E et al (2020) Pd/IGZO/p^+-Si synaptic device with self-graded oxygen concentrations for highly linear weight adjustability and improved energy efficiency. ACS Appl Electron Mater 2:2390–2397
21. Kumar A, Herng TS, Zeng K, Ding J (2012) Bipolar charge storage characteristics in copper and cobalt co-doped zinc oxide (ZnO) thin film. ACS Appl Mater Interfaces 4:5276–5280
22. Mandal R, Mandal A, Mitra A, Som T (2022) Emulation of biosynaptic behaviours in copper-doped zinc oxide memristors: a nanoscale scanning probe microscopic study. Appl Surf Sci 606:154860
23. Younas M, Xu C, Arshad M et al (2017) Reversible tuning of ferromagnetism and resistive switching in ZnO/Cu thin films. ACS Omega 2:8810–8817
24. Son JY, Shin YH (2008) Direct observation of conducting filaments on resistive switching of NiO thin films. Appl Phys Lett 92:222106

Publisher's Note Springer Nature remains neutral with regard to jurisdictional claims in published maps and institutional affiliations.

Springer Nature or its licensor (e.g. a society or other partner) holds exclusive rights to this article under a publishing agreement with the author(s) or other rightsholder(s); author self-archiving of the accepted manuscript version of this article is solely governed by the terms of such publishing agreement and applicable law.